ALEPH 89-2
EMCAL 89-1
M. Bardadin et al.
22.12.88

Electromagnetic calorimeter response to muons and non-interacting pions

Maria Bardadin-Otwinowska[1)], Denis Bernard[2)], Youssef Saadi[1)]

[1)] Laboratoire de Physique Corpusculaire, Clermont-Ferrand

[2)] Ecole Polytechnique, Palaiseau

Abstract

The response of the ALEPH electromagnetic calorimeter to minimum ionising particles is studied using data taken with pion and muon beams.

Mean values and the fluctuations of the signal induced by non-interacting particles are studied. A relativistic rise in the ionisation is observed in the energy range 10 to 55 GeV.

The signal per unit of energy deposited in the calorimeter is found to be about 1.5 times larger for minimum ionising particles than for electron showers .

Introduction

The relative response to electromagnetic showers and to minimum ionising particles, called the e/mip ratio, is an important intrinsic property of a sampling calorimeter.

The Aleph electromagnetic calorimeter has a high-Z (lead) absorber and therefore minimum ionising particles are expected to produce stronger signals than electrons depositing the same energy [1], i.e. $e/mip < 1$.

The e/mip ratio is one of relevant parameters determining the calorimeter response to hadronic showers. However, the electron/hadron ratio depends also on other effects which are poorly known: neutron and soft gamma detection efficiencies, binding energy losses and possible saturation effects. They decrease the detected hadron signal and contribute towards a better compensation (e/h=1); they could even make the ratio e/h exceed 1. Experimentally, the ratio e/π for the electromagnetic calorimeter is greater than 1 and depends on the pion energy; this result was found from the analysis of the combined response of the electromagnetic and hadronic calorimeters [2].

The behaviour of the electromagnetic showers in ECAL is well known from abundant experimental data and detailed EGS simulations [3]. The response to charged particles is studied in the present note, using data taken with incident muons and non-interacting pions. The incident energies vary between 10 and 55 GeV, this range corresponds to the region of the relativistic rise of ionisation. The term 'nips' is used here for the non-interacting particles studied in order to distinguish them from fictitious 'mips' (minimum ionising particles). Their properties are deduced by an extrapolation of the nips' data.

All measured ADC signals are expressed in energy units calibrated using electron shower data. An electron of known energy E_e, which in this test run was equal to 10 GeV, induces a total ADC signal A_e. The 45 gas layers of the calorimeter are identical,

whereas the thickness of the passive material per detection plane, measured in radiation length units, is larger in stack 3 than in stacks 1 and 2 by a factor 1.934. Therefore the contribution of stack 3 to A_e was weighted by this factor. A measured signal A is converted to the calibrated signal E according to the formula:

$$E = A\frac{\mathrm{E}_e}{A_e}.$$

In this note, the symbol E always means the calibrated signal while the energy deposited in the calorimeter is denoted by E. Normally, the calibration includes the stack-3 correction for the measured signal. However, when individual plane signals induced by a nip are studied, no such correction is applied. The signals are then expected to be on the average the same in all planes.

After a description of the experimental set-up, the method of selecting non-interacting pions is explained.

The variation of the signal induced by nips with the particle energy is measured and compared with the predictions of the Bethe-Bloch formula for the mean energy loss in the gas and in the passive material. The ratio e/nip is determined from the data and extrapolated to e/mip.

The distributions of the stack signals are presented and fitted with an empirical function. The fluctuations of the energy deposited in one gas layer of the ECAL prototype were discussed in [4]. Here, results obtained for the module are presented and the validity of application of the Landau predictions is discussed.

The Experimental Set-up

A barrel module of the electromagnetic calorimeter was placed in the X7 beam line of the CERN SPS West Hall for the 1986 test period. The detector was filled with a mixture of 80% Xenon and 20% CO_2 by volume. It was exposed to the pion beams of 10, 25 and

50 GeV and a muon beam of 55 GeV. Shortly after each run, a 10 GeV electron run was taken for calibration. A small correction for the drift of the gain of the calorimeter was added.

All beam particles passed through the simulated e^+e^- intersection point, and were therefore incident on the detector at various angles.

The trigger and the shape of the beam were defined with a set of scintillators used in coincidence. Furthermore a spectrometer provided a measure of the momentum of the incident particle and a hodoscope made of four wire chambers provided its position and angle at the entrance of the module. The spectrometer and the hodoscope were also used to select events with only one track entering the detector.

The Selection of Nips

The first step of the analysis is the selection of the nip events from the data themselves. The method is described in this section and illustrated in Figs 1-6, which refer to the 10 GeV pion data. As the muon beam was contaminated with hadrons, the same selection criteria were also applied to muons.

Interacting hadrons and nips clearly have different signatures. Fig. 1 shows the distribution of the total calibrated signal, i.e. of the sum of all the wire plane signals, with the stack 3 correction included. It shows a peak at a few hundred MeV due to nips and a broad spectrum from hadronic showers (the peak at 10 GeV reveals some electron contamination).

Longitudinal profiles will now be investigated in detail. The signal from one wire plane for one event is denoted by δE, and the distribution of δE against plane number gives the longitudinal profile.

Fig. 2 and Fig. 3 present a typical profile for each of a nip and a pion-induced hadronic shower, respectively. For strongly interacting hadrons, the signal is generally higher. Their longitudinal profile shows large clusters of fired planes following a primary interaction in the module. The nips deposit only a few hundred MeV in the module, but the energy distribution has a high-energy tail due to Landau fluctuations. A simple cut could bias the data sample. Although the energy deposited by nips in one plane may be high, the longitudinal profile typically does not present any clustering, contrary to the behaviour of interacting hadrons. This property is used to elaborate a safe and powerful selection method. The procedure is iterative and applies alternatively a 'global' and a 'local' cut on the data.

First the truncated sum, t, of the n=38 smallest signals out of the 45 signals was calculated. The value of n was tuned so that the distribution of t for uncorrelated nips (defined in the following) is gaussian. The distribution of t for the initial sample of all events is plotted in Fig. 4. The r.m.s value of the peak due to nips, σ_t, amounts to about 30% of the mean $< t >$. A 3-standard-deviation cut is applied on the value of t in each iteration.

A 'local' cut is also applied. In an event, all sets of 8 consecutive wire planes are considered and for each set the number of planes fired above 5 times $< t > /n$ is counted. The maximum value of this number for each event is retained, and is denoted by k. The distribution of k for the initial sample (before any cut on t) is plotted in Fig. 5. Events with k greater than 4 are rejected. An additional cut was introduced on the four last planes to reject the events presenting a primary interaction in that region.

In each step, the values of $< t >$ and σ_t are recalculated, and the cuts on t and k applied. Stability was reached after 2 to 3 iterations. The distributions of t and k for the selected nip events are presented in Figs 4 and 5. The arrows represent the final cuts.

As a check of the method a sample of 'uncorrelated' nips was generated by reshuffling the nip events in blocks of 45. Within each block, the wire planes were permuted so that

the first uncorrelated event is formed by taking the plane i of the event number i , i=1,..,45, the second one by taking the plane i of the event i+1, etc. The selection cuts were applied again on the uncorrelated sample with an efficiency close to 1.

The mean longitudinal profile of the signal (Fig. 6) appears then to be flat within statistical errors for the selected sample of nips. The residual contamination of interacting pions, which would lead to an increase of the signal with increasing plane number, is therefore low.

The mean signal per plane

After the selection, the mean signal per plane, δE, is calculated for the nips. The data taken at various incident angles are combined after multiplication by the cosine of the incident angle. It has been checked that no systematic dependence of the signal on the incident angle was observed between 0 and 39 degrees. The results are listed in Table 1 and plotted as a function of the incident particle energy in Fig. 7.

Table 1. Mean signal per wire plane, calibrated with electron showers, for non-interacting particles.

Particle	E_{beam} (GeV)	$< \delta E >$ (MeV)	Statistical error (MeV)
π	10	6.55	0.06
π	25	6.87	0.02
π	50	7.24	0.02
μ	55	7.48	0.02

The result at 10 GeV is consistent with the value 6.42 MeV measured for non-interacting pions at 5 and 10 GeV in the prototype [5]. A relativistic rise of 14 % is observed between 10 and 50 GeV.

Comparison of the data with a simulation

The average calibrated signal induced by nips in one layer can be written in the form:

$$E_{nip} = (A_{nip}/A_e) \cdot \mathrm{E}_e^{pas} = (\mathrm{E}_{nip}^{gas}/\mathrm{E}_e^{gas}) \cdot \mathrm{E}_e^{pas} = \mathrm{E}_{nip}^{gas}/f_e.$$

f_e is the sampling fraction for electron showers, defined as the ratio of the energies deposited by an electron shower in the active and passive materials:

$$f_e = \mathrm{E}_e^{gas}/\mathrm{E}_e^{pas}.$$

The value of f_e is known from the EGS simulation [3] of the electron showers in the calorimeter prototype. The prototype consisted of 55 detection planes identical to those of stacks 1 and 2 of the module. The ratio f_e was found to be constant for the showers generated at several energies between 20 MeV and 50 GeV ; this result is in agreement with the experimentally observed linearity of the calorimeter response with the electron energy. The numerical value of f_e for the Xe/CO_2 mixture is

$$f_e = 0.323 \cdot 10^{-3}.$$

The energy deposited by a nip in the gas, E_{nip}^{gas}, is calculated from the Bethe- Bloch formula with Sternheimer's density correction [6,7]. The geometry of the module is described in Ref [8]. The calculation is done for pions normally incident at the calorimeter face. The mean path in the gas is taken equal to 90% of the cell depth since in 10% of cases the particle traverses a rib. The $d\mathrm{E}/dx$ formula and the values of the numerical constants used are given in the Appendix.

The predicted signal, $\mathrm{E}_{nip}^{gas}/f_e$, is compared with the data in Fig. 7. The upper curve represents the unrestricted energy loss. The lower one was calculated from the $d\mathrm{E}/dx$ formula adjusted to pass through the data points by putting a cut-off on W_{max}.

Determination of the e/nip Ratio

The total calibrated calorimeter signal is plotted in Fig. 8 as a function of the pion energy. It is equal to the sum of all 45 planes, with the stack-3 correction taken into account. The curve represents the energy loss in the passive material calculated from the unrestricted dE/dx formula. The calibrated signal is considerably larger than the energy really deposited by a nip traversing the calorimeter.

As a measure of the relative response of a calorimeter to electrons and ionising particles, the parameter e/nip is used. It is defined as the ratio of the corresponding sampling fractions

$$\frac{e}{nip} = \frac{f_e}{f_{nip}},$$

where

$$f_{nip} = \mathrm{E}^{gas}_{nip} / \mathrm{E}^{pas}_{nip}.$$

Unlike the sampling fraction for electron showers, which is energy independent, f_{nip} varies with energy since the relativistic rise is different in the gas and in the passive material. One obtains

$$\frac{e}{nip} = \frac{f_e \cdot \mathrm{E}^{pas}_{nip}}{\mathrm{E}^{gas}_{nip}} = \frac{\mathrm{E}^{pas}_{nip}}{E_{nip}}.$$

E^{pas}_{nip} is the total energy deposit in the passive material of the calorimeter, already shown in Fig. 8, and E_{nip} is the total calibrated signal, i.e. the one-plane signal of Fig. 7 multiplied by 33+12*1.934 = 56.2. e/nip is calcutaled using the experimental data points between 10 and 55 GeV and the variation is extrapolated to lower energies using the adjusted curve of Fig. 7. The results are plotted in Fig. 9. At 55 GeV

$$\frac{e}{nip} = .70,$$

and for minimum ionising particles, by extrapolation, $e/mip = .62$.

Summarizing, a signal induced by a n.i.p. and calibrated with electrons overestimates the energy deposited in the passive material by about 50%.

Stack signals

In real events, the wire signals will generally not be available for individual particles and therefore it is more practical to study the stack signals E_1, E_2 and E_3. In this analysis, the stack signal is defined as a sum of the wire signals, multiplied by the cosine of the incident angle i. The criteria previously used to select nips are now replaced by the following more crude but simpler cuts:

$$E_1 < 200\ MeV$$

$$E_2 < 400\ MeV$$

$$E_3 < 200\ MeV.$$

The sample of nips satisfying the cuts is practically identical to the previous selection. In particular, the mean values of the calibrated signal remain unchanged.

The distributions of the stack signals induced by muons of 55 GeV momentum are plotted in Figs 10 a, b and c. Fig 10 d shows the distribution for the sum of the three stacks. The stack-3 data in Fig. 10 c and their contribution to the total signal in Fig.10 d are weighted by the factor 1.934. The upper scale indicates the signal per layer. The plots were drawn keeping the upper scale identical for the four distributions, in order to visualise the dependence of the shape on the number of contributing layers.

Each of the distributions was fitted with the empirical formula

$$f(\Delta) = C \cdot \exp[-0.5(\Delta + \exp(-\Delta)],$$

where

$$\Delta = \frac{(E - E_0)}{S}.$$

The parameter E_0 gives the position of the maximum of the distribution and S is a measure of its width. They were determined by the fit and the obtained values are listed in Table 2.

Table 2. Results of the fits of the distributions of the stack signals

	Number of layers	E_0 (MeV)	S (MeV)
stack 1	10	50.9	15.5
stack 2	23	134.1	31.3
stack 3	12	127.0	36.2
all stacks	45	348.4	55.8

One notes that the shape of the distribution of the average signal per layer depends on the number of layers N. The position of the maximum E_0/N increases with N and the width parameter S/N decreases. The r.m.s. values, σ, are consistent with the relationship

$$\frac{\sigma}{\sqrt{N}} \simeq 11.6\,\mathrm{MeV}$$

.

The fluctuations of the stack signals weighted by cos$i$ may still depend on i. The statistics is unsufficient to study this effect. The presented results are averaged over the range 0 to 39 degrees.

Fluctuations

The distribution of the signal read in a single plane, δE, presents a typical Landau shape (Fig 11). The tail of the distribution is expected to follow a $(\delta E)^{-\alpha}$ law with α equal to 2, for a pure Landau term. The experimental variation of α with δE was determined by a series of fits to blocks of 8 successive data points; the obtained values of α are plotted in

Fig. 12 versus the central value of the δE interval used in the fit. The figure shows that α is close to 2 over one order of magnitude of δE (10-100 MeV).

The energy lost by the incident particle in the gas is not necessarily locally deposited; if the range of a delta electron is larger than the distance to the wall, then a part of the electron energy is absorbed in the passive material and does not contribute to the measured signal. According to the range-energy relationship

$$\mathrm{E} = \left(\frac{R.\rho}{0.71}\right)^{.58},$$

where E is in MeV, R in cm, and ρ the density in g/cm^3, this occurs in Xenon for electrons of energy greater than 27 keV , taking the depth of one cell, R=.32 cm, as a typical distance. The corresponding calibrated signal is about 100 MeV. Harder delta rays can leave the gap and therefore α rises for δE greater than this value.

Thus the unrestricted energy loss formula is not appropriate to describe the fluctuations of the signal in the gas, nor is the formula with a sharp cut-off of the energy transfer. However the variation of the mean signal with energy (Fig. 7) is correctly described by the formula with an effective cut-off on W_{max}.

Appendix

The average energy loss is calculated from the Bethe-Bloch formula modified by the density correction [6]:

$$\frac{1}{\rho} \cdot \frac{dE}{dx} = \frac{D}{\beta^2} [B + ln2 + 2\ ln(\beta\gamma) + ln\, W_{max} - 2\beta^2 - \delta],$$

where

$$D = .1536\, Z/A \ \ MeV.cm^2/g,$$

$$B = ln\, \frac{m_e \cdot 10^6}{I^2},$$

$$W_{max} = (2m_e\beta^2\gamma^2c^2) \Big/ \left[1 + 2\gamma\frac{m_e}{M} + \left(\frac{m_e}{M}\right)^2\right],$$

A and Z are the mass and charge numbers, I is the mean ionisation potential in eV, W_{max} is the maximum energy transfer from the incident particle of mass M to an atomic electron, and m_e is the electron mass.

The density correction δ partly suppresses the relativistic rise. It is parametrized as a function of the variable X:

$$X = \log_{10}(\beta\gamma) = 2\, ln\, (\beta\gamma)/4.606,$$

$$\delta = 0 \qquad \text{for } X < X_0,$$

$$\delta = 4.606\ X + C + a\ (X_1 - X)^m \qquad \text{for } X_0 < X < X_1,$$

$$\delta = 4.606\ X + C \qquad \text{for } X > X_1.$$

The values of the constants are listed in Tables 3 and 4 for the materials present in the calorimeter. They are taken from Ref [7] for solids and calculated according to the formulae given in [6] for the mixture of 80 % of Xenon and 20 % of CO_2 by volume in normal conditions.

Table 3. Material constants

Material	Density ρ (g/cm^3)	Ionisation Potential (eV)	D (MeVcm^2/g)	B
Pb	11.35	823	0.0608	13.53
Al	2.7	166	0.0740	16.73
PVC	1.38	108	0.0787	17.59
Xe/CO_2	4.7610^{-3}	403	0.0642	14.96

Table 4. Density correction parameters

Material	C	X_0	X_1	a	m
Pb	−6.2018	0.3776	3.8073	0.0936	3.1608
Al	−4.2395	0.1708	3.0127	0.0802	3.6345
PVC	−4.0532	0.1559	2.9415	0.1244	3.2104
Xe/CO_2	−12.566	2.0154	5.0154	0.1216	3.0000

References

1. R.Wigmans, NIM A259 (1987) 389.
2. F.Combley, M.Dinsdale, M.Pepe, M. de Palma, L.Silvestris, ALEPH 88-188.
3. J.Prat, Thesis, Université Clermont-Ferrand, 1985.
4. D.Bernard, Thesis, Université Orsay-Paris XI, 1984.
5. M.Bardadin-Otwinowska, J.Badier, ALEPH 87-9.
6. R.M.Sternheimer and R.F.Peierls, Phys. Rev. B3 (1971) 3681.
7. R.M.Sternheimer, M.J.Berger, S.M. Seltzer, Atomic Data and Nuclear Data Tables, 30 (1984) 261.
8. B.Bloch-Devaux, ALEPH 86-67.

Figure Captions

Figure 1. The distribution of the signal induced by the 10 GeV pions.

Figure 2. The longitudinal profile of a typical interacting-pion event.

Figure 3. The longitudinal profile of a typical nip event.

Figure 4. The distributions of the truncated sum of the wire plane signals, t, for the initial sample of all events and for the events accepted as nips.

Figure 5. The distribution of k (as defined in the text) for the initial sample of all events and for the events accepted as nips.

Figure 6. The mean longitudinal profile of nips.

Figure 7. The mean signal per layer induced by a pion or muon as a function of its energy. The upper curve is the prediction assumung unrestricted energy loss, the lower one is a parametrisation obtained by putting a limit on W_{max}.

Figure 8. The mean total calibrated signal as a function of the energy of the incident particle. The curve is the energy loss in the calorimeter calculated from the $d\mathrm{E}/dx$ formula.

Figure 9. The ratio f_e/f_{nip} as a function of the energy of the incident particle

Figure 10. The distribution of the calibrated nip signals in stacks 1,2 and 3 and of the total signal (sum of the three stacks).

Figure 11. The distribution of the signal induced by a nip in a single plane.

Figure 12. The variation of the exponent α of the Landau tail with the energy region used for the fit.

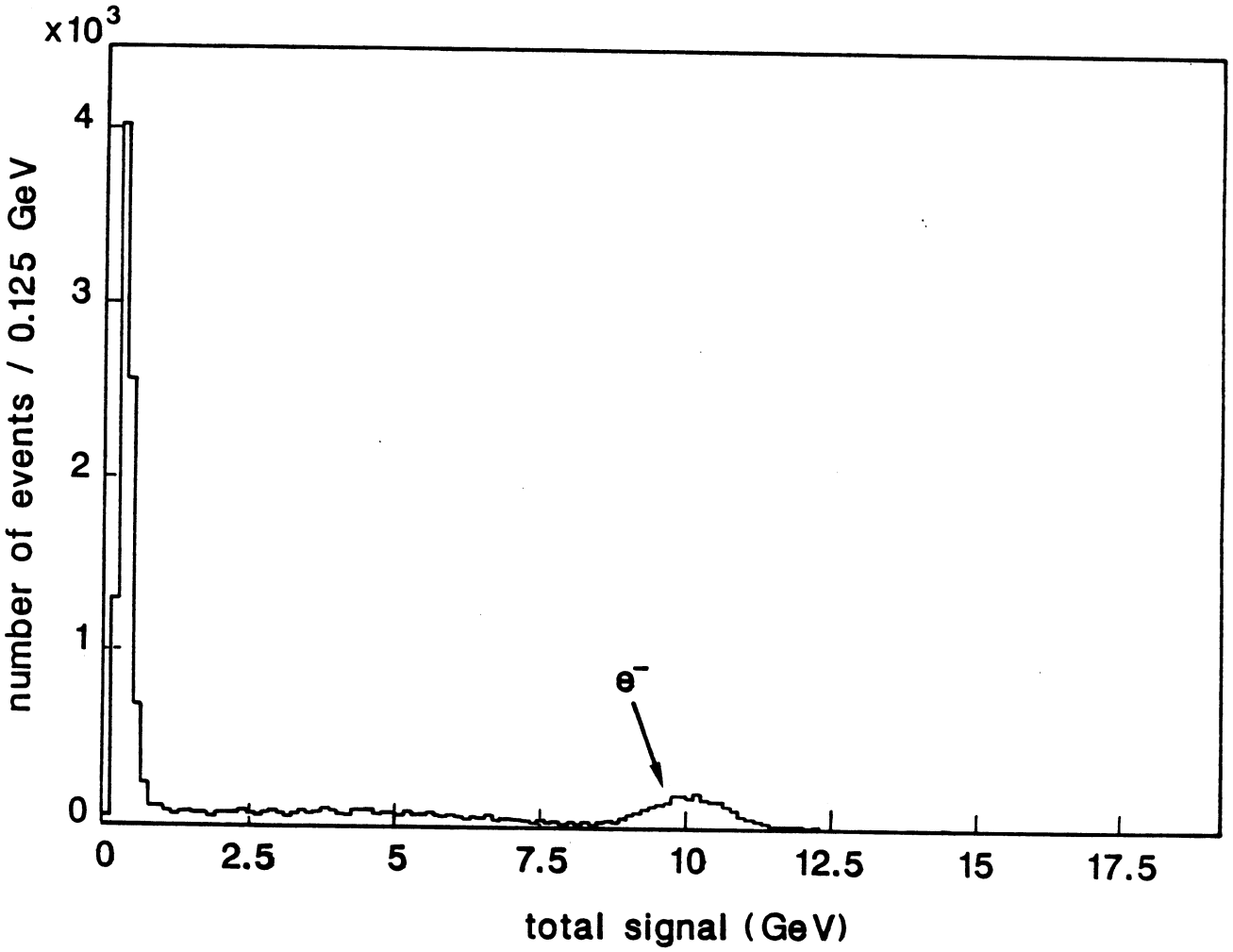
x10^3
4
3
2
1
0
number of events / 0.125 GeV
e⁻
0
2.5
5
7.5
10
12.5
15
17.5
total signal (GeV)

Fig.1

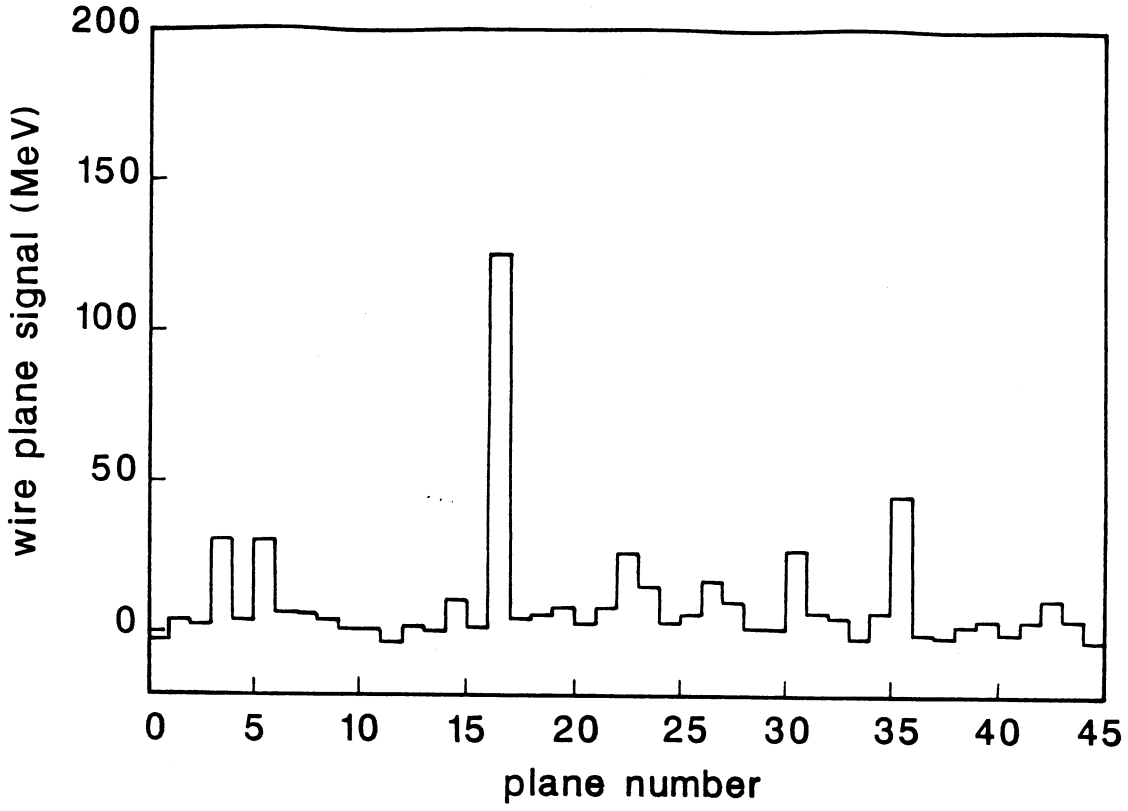
200
150
100
50
0
wire plane signal (MeV)
0
5
10
15
20
25
30
35
40
45
plane number

Fig.2

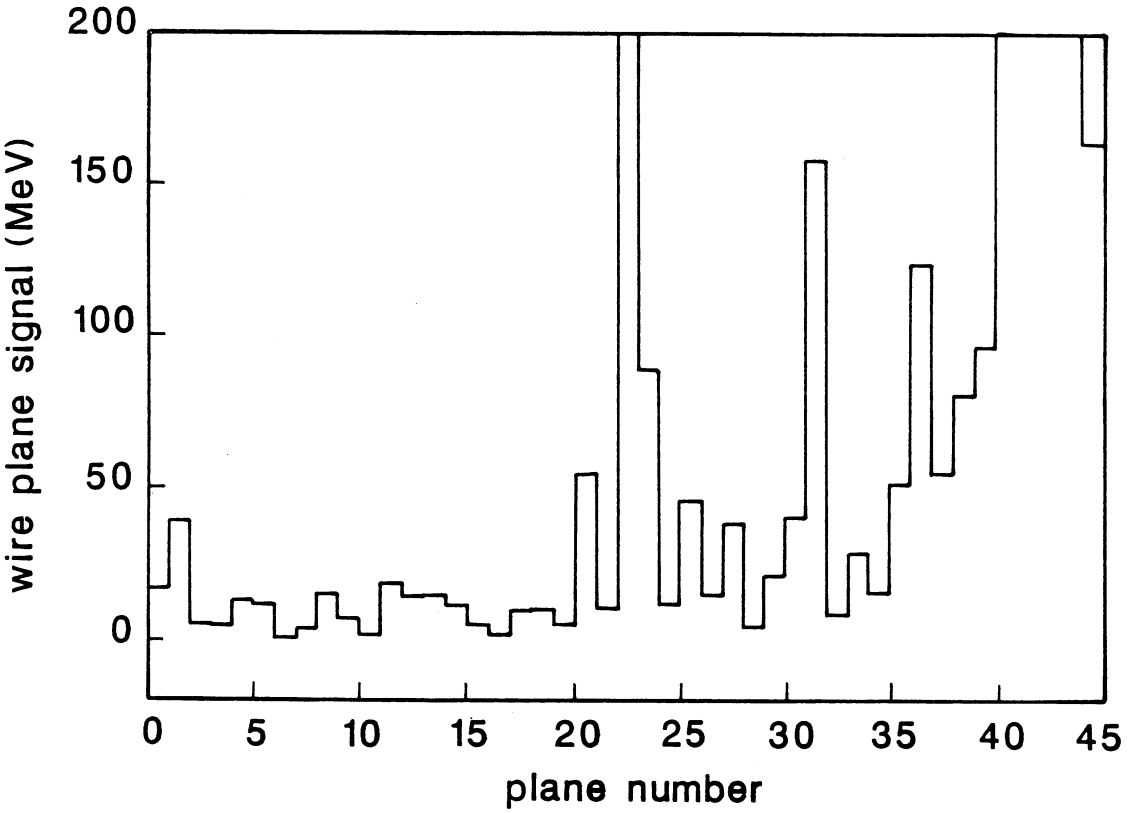
200
150
100
50
0
wire plane signal (MeV)
0
5
10
15
20
25
30
35
40
45
plane number

Fig.3

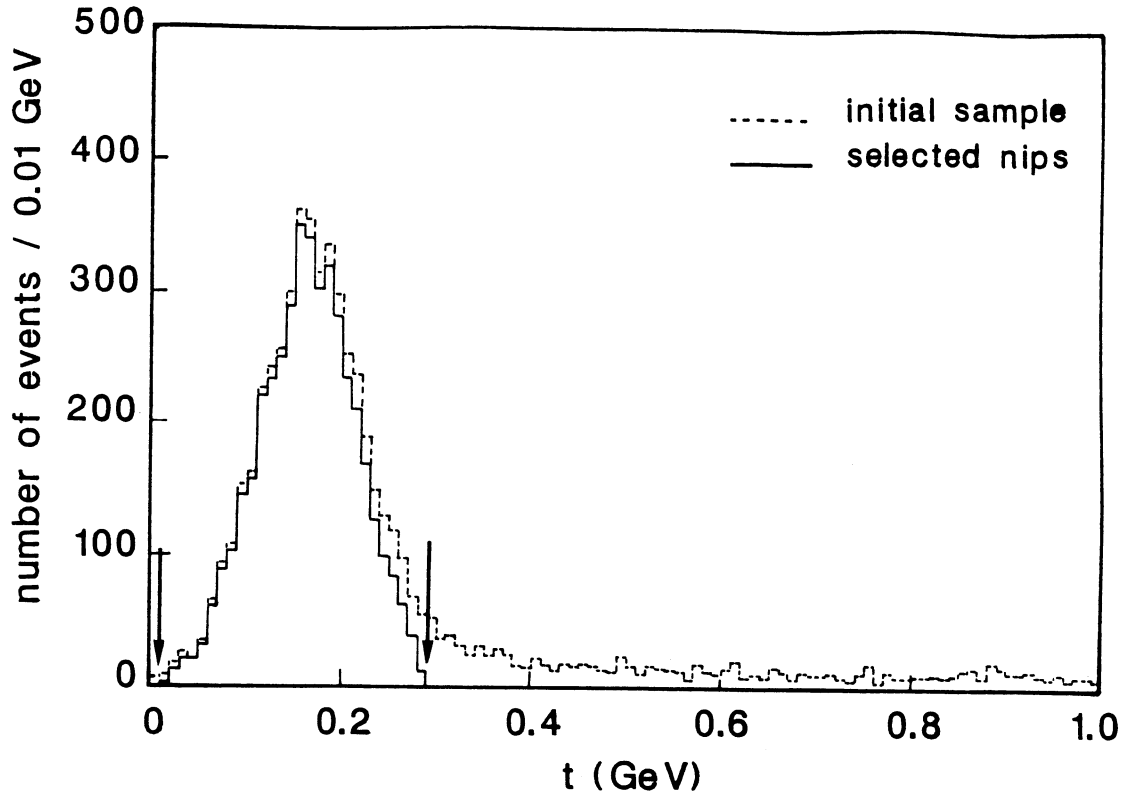
500
400
300
200
100
0
number of events / 0.01 GeV
initial sample
selected nips
0
0.2
0.4
0.6
0.8
1.0
t (GeV)

Fig.4

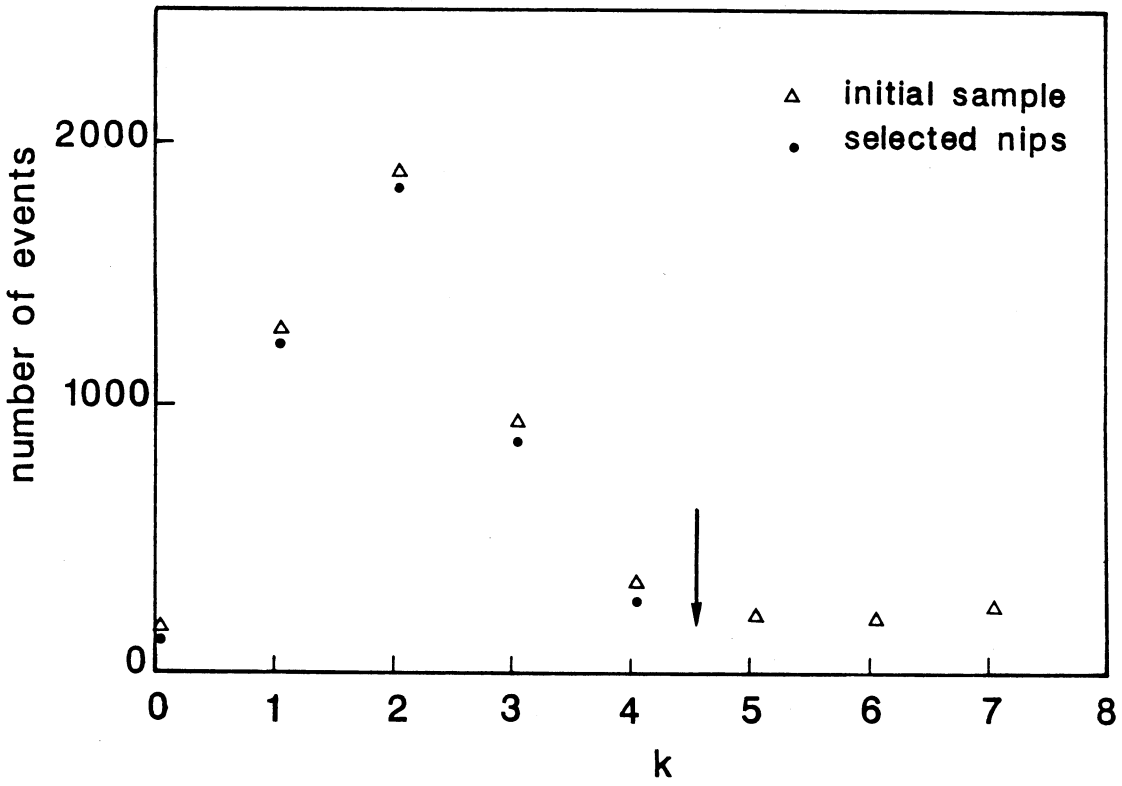
2000
1000
0
number of events
initial sample
selected nips
0
1
2
3
4
5
6
7
8
k

Fig.5

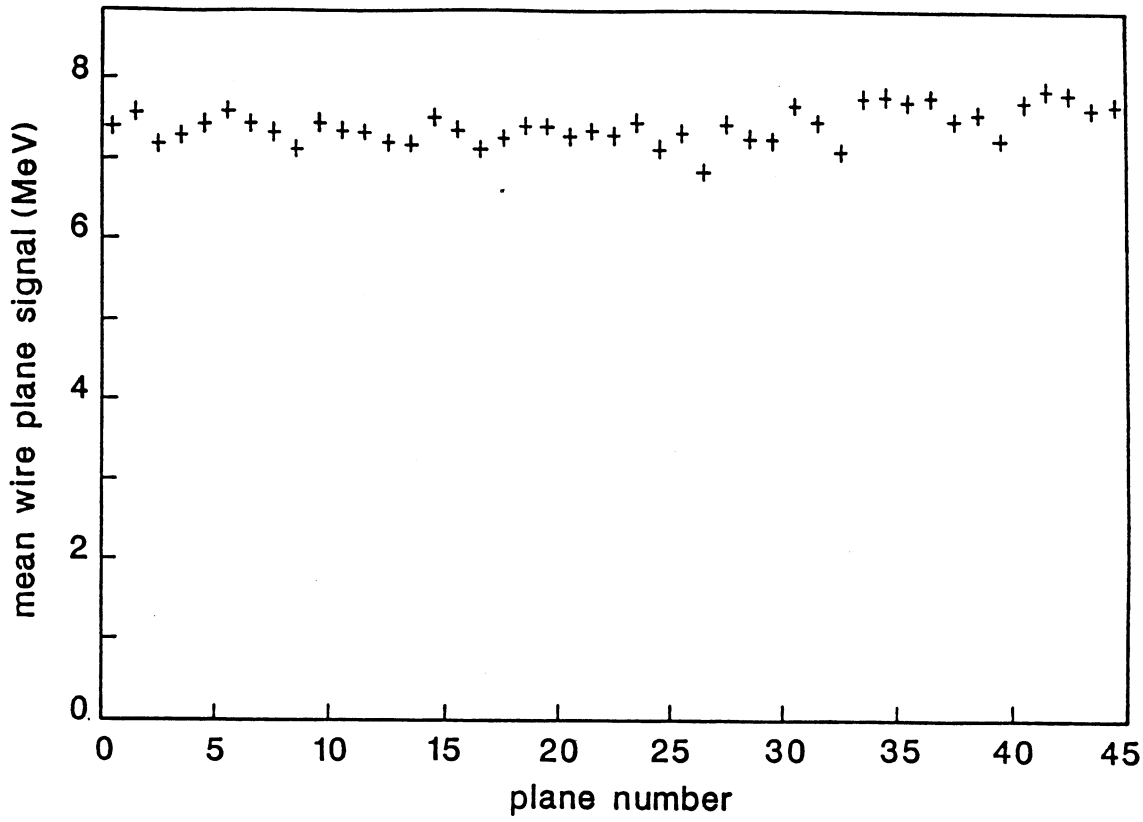
mean wire plane signal (MeV)
0
2
4
6
8
0
5
10
15
20
25
30
35
40
45
plane number

Fig.6

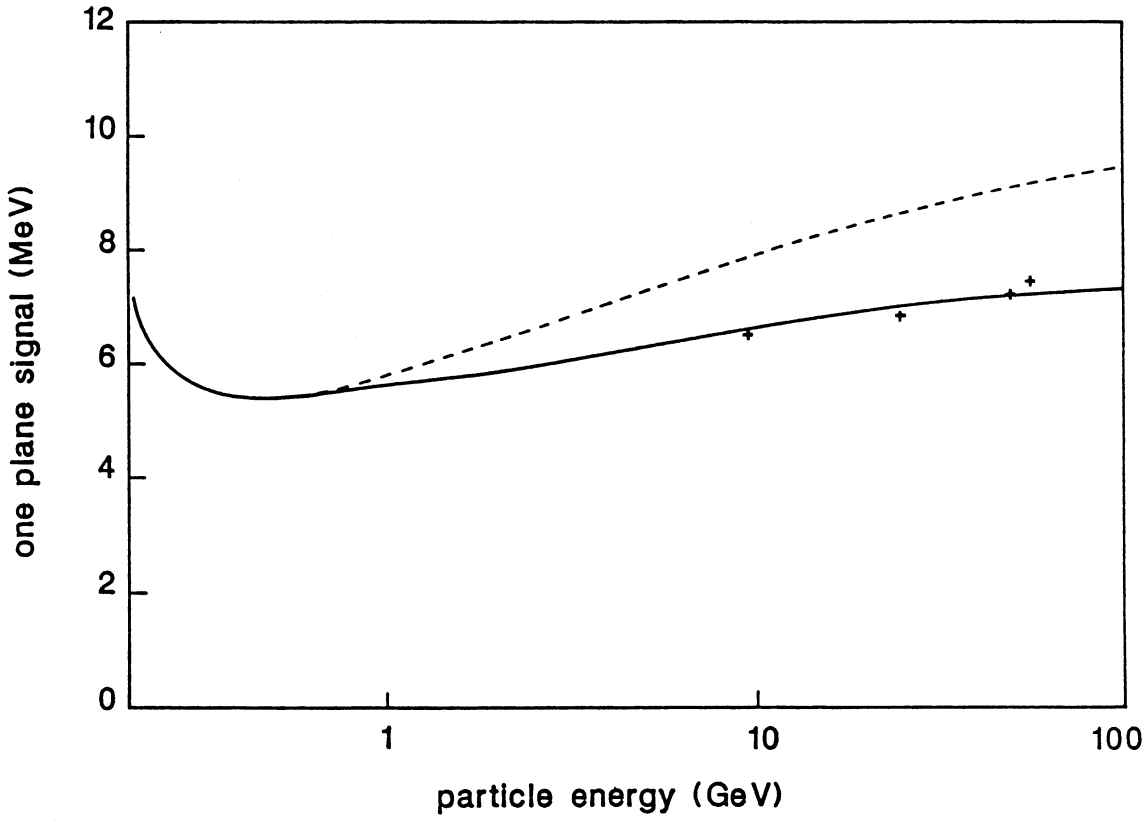
one plane signal (MeV)
0
2
4
6
8
10
12
1
10
100
particle energy (GeV)

Fig.7

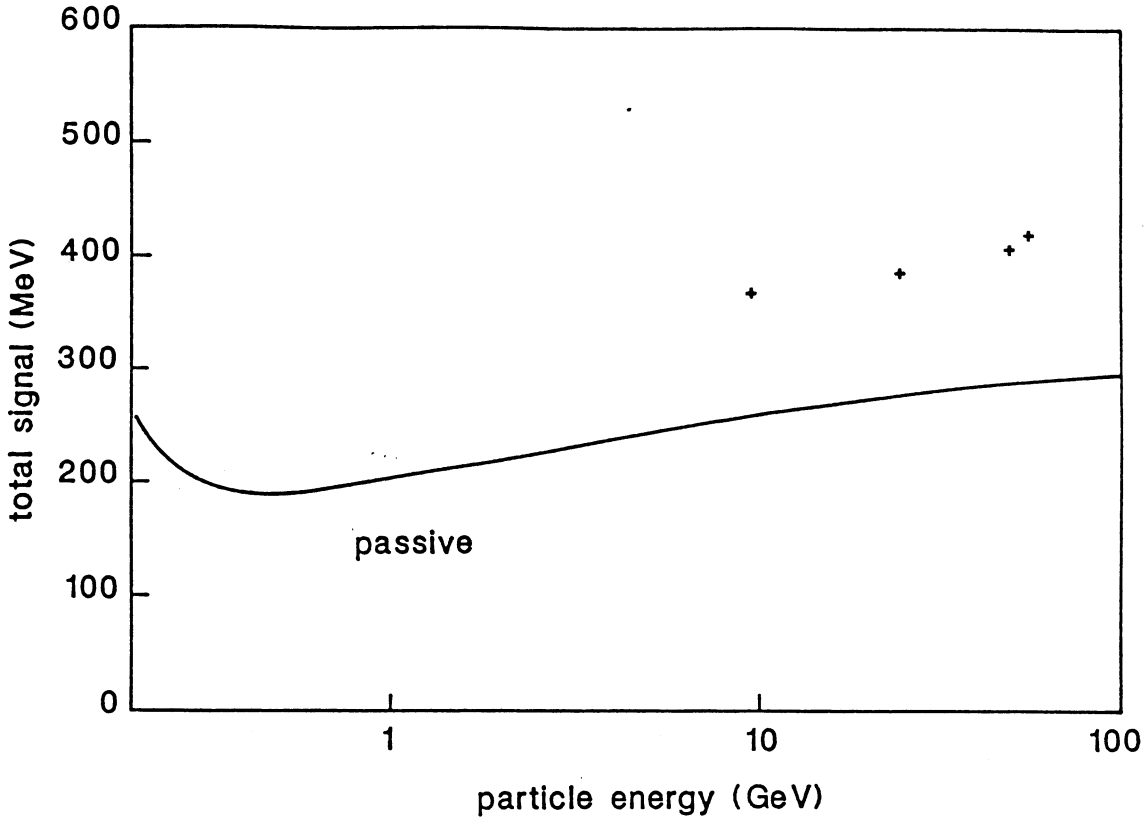
600
500
400
300
200
100
0
total signal (MeV)
passive
1
10
100
particle energy (GeV)

Fig.8

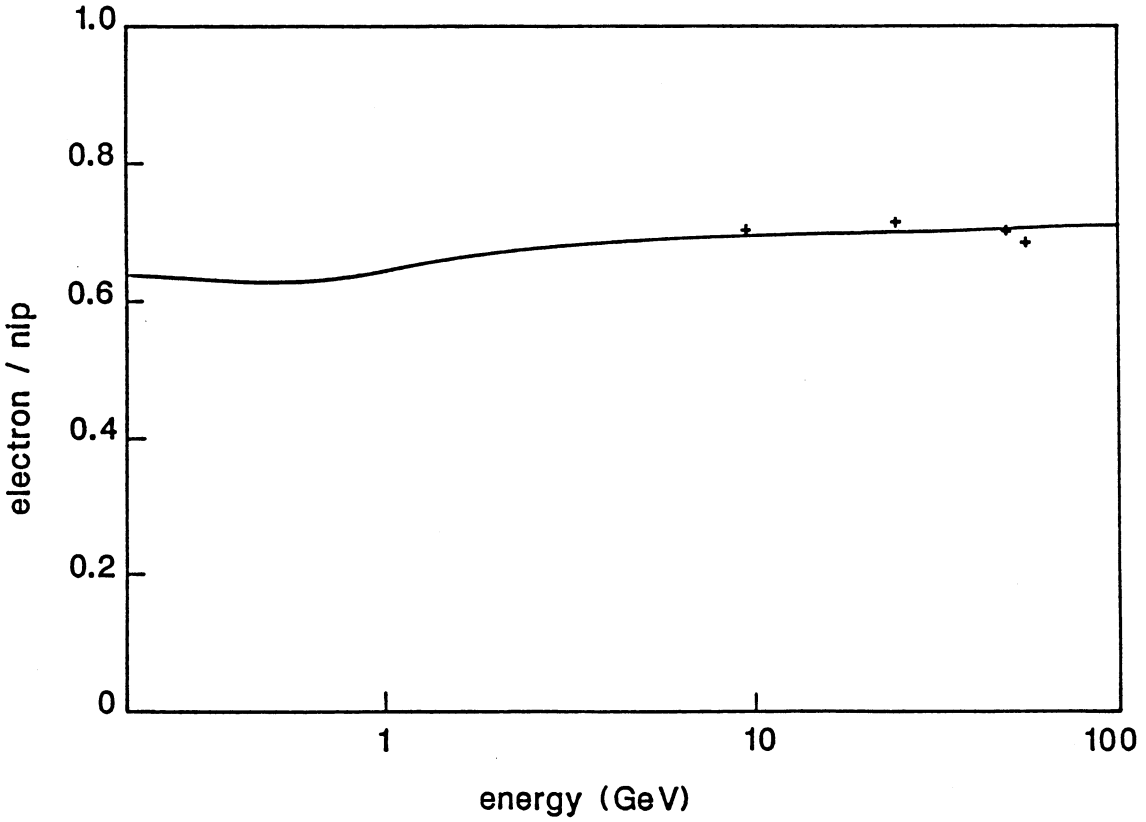
1.0
0.8
0.6
0.4
0.2
0
electron / nip
1
10
100
energy (GeV)

Fig.9

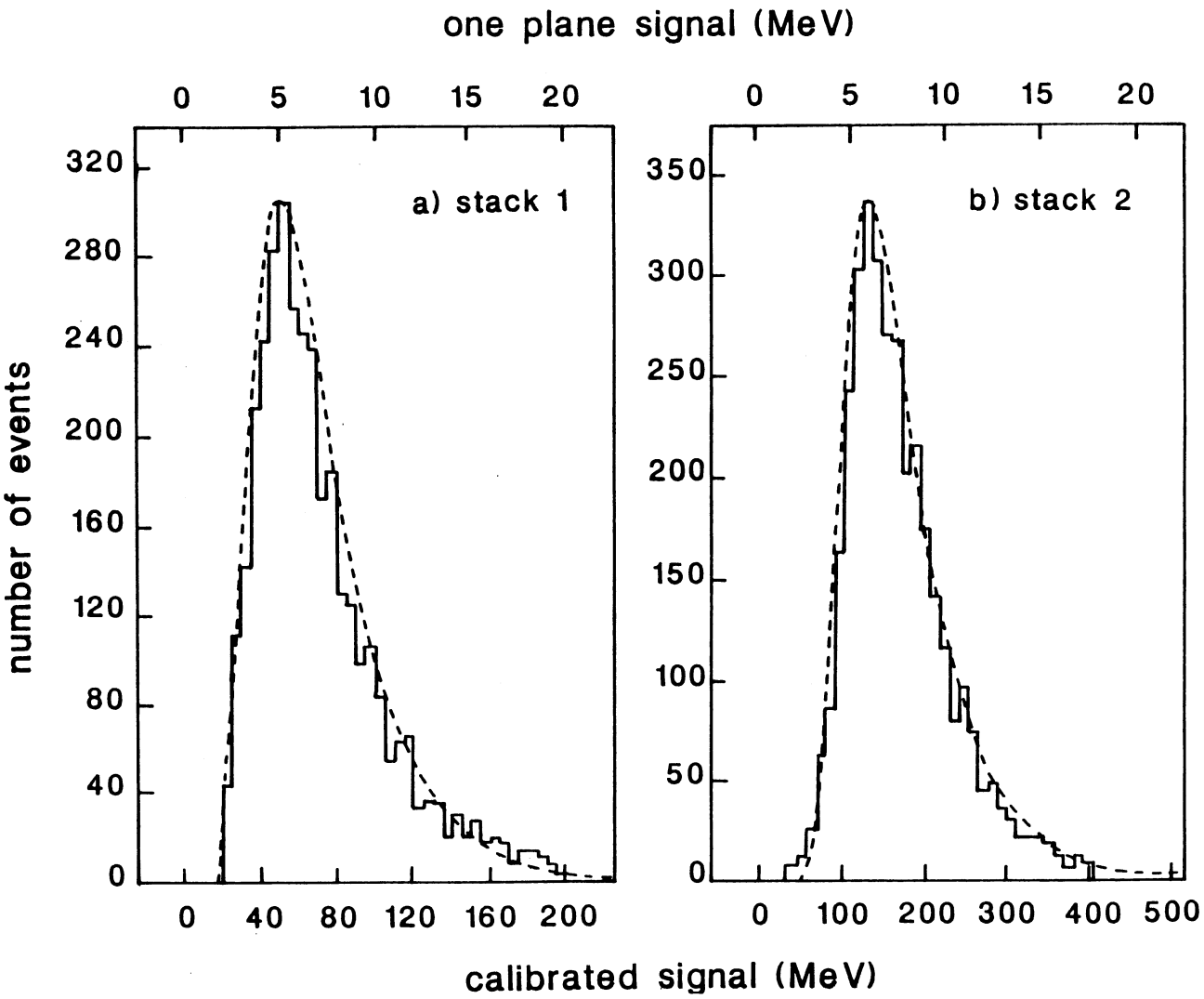
one plane signal (MeV)
0 5 10 15 20
a) stack 1
b) stack 2
number of events
320
280
240
200
160
120
80
40
0
350
300
250
200
150
100
50
0
0 40 80 120 160 200
0 100 200 300 400 500
calibrated signal (MeV)

Fig.10

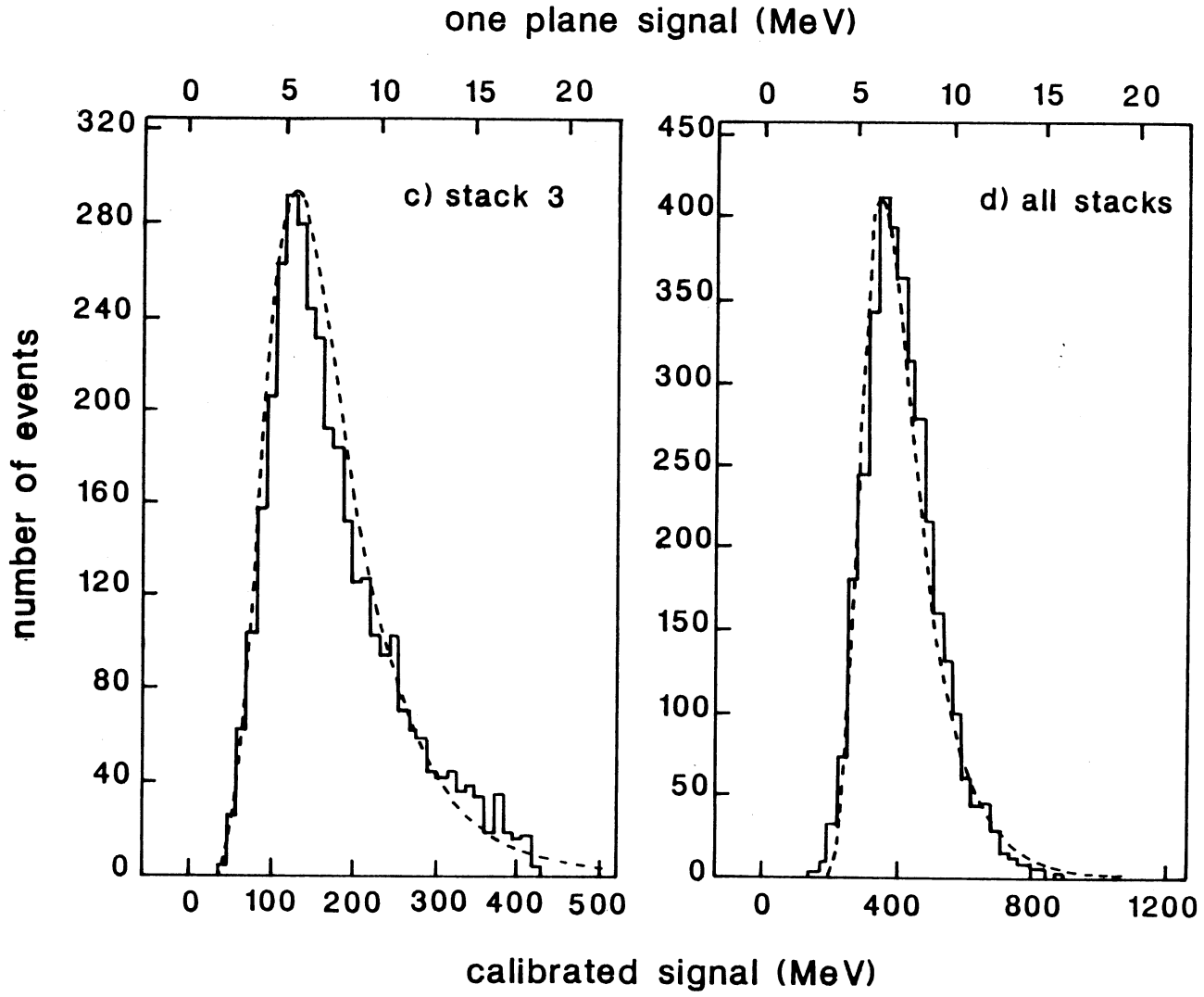
one plane signal (MeV)
0
5
10
15
20
320
280
240
200
160
120
80
40
0
c) stack 3
0
100
200
300
400
500
450
400
350
300
250
200
150
100
50
0
d) all stacks
0
400
800
1200
number of events
calibrated signal (MeV)

Fig.10

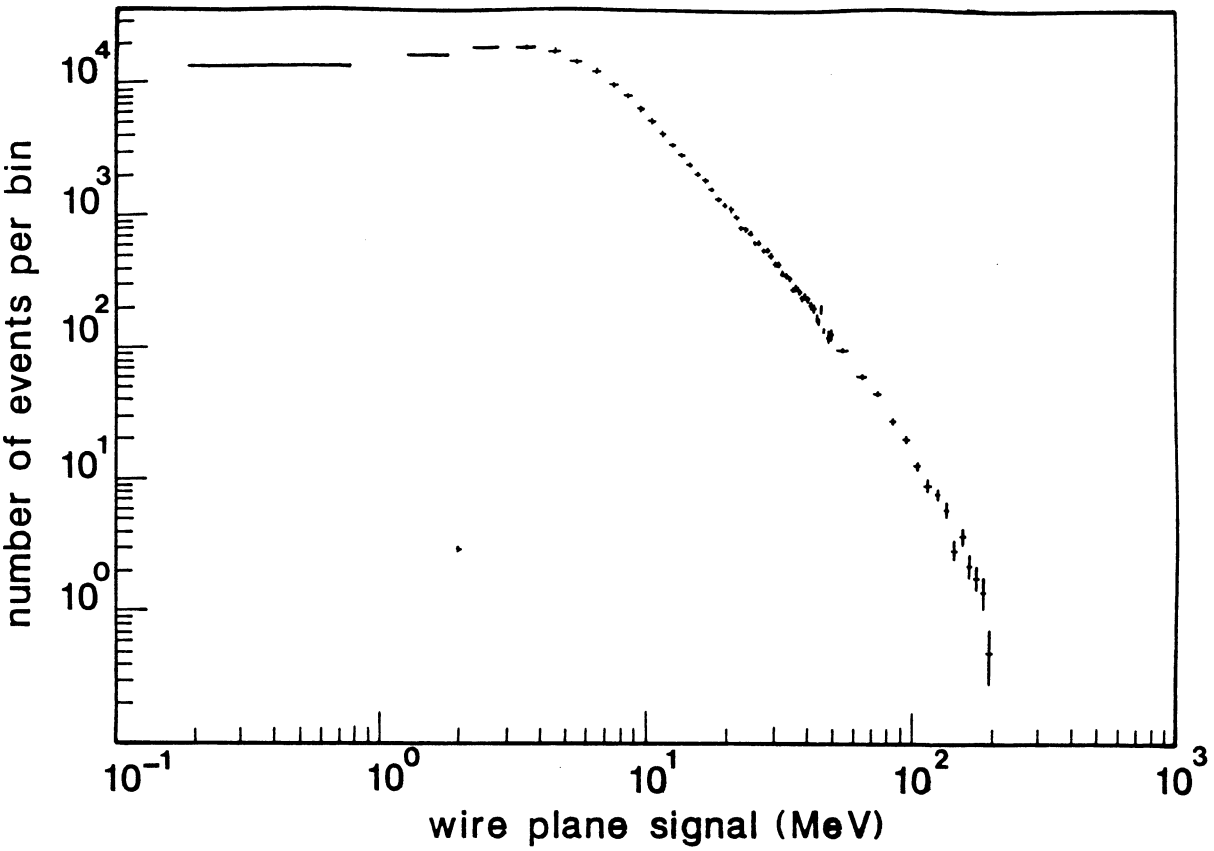
number of events per bin
10^4
10^3
10^2
10^1
10^0
10^{-1}
10^0
10^1
10^2
10^3
wire plane signal (MeV)

Fig.11

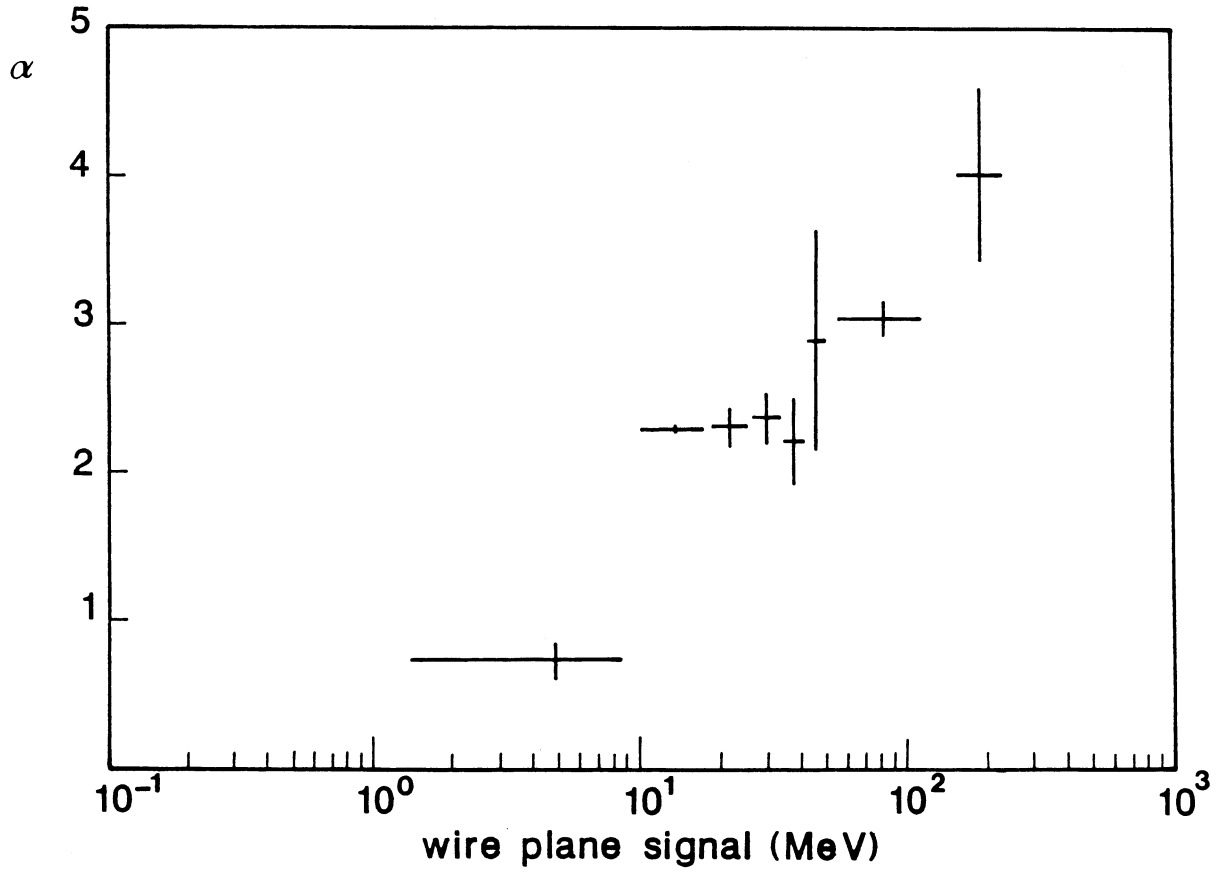
α
5
4
3
2
1
10^{-1}
10^0
10^1
10^2
10^3
wire plane signal (MeV)

Fig.12